Supplementary Materials for

The [4Fe4S] Cluster of Human DNA Primase functions as a Redox Switch Using DNA Charge Transport

Elizabeth O'Brien, Marilyn E. Holt, Matthew K. Thompson, Lauren E. Salay, Aaron C. Ehlinger, Walter J. Chazin, Jacqueline K. Barton

correspondence to: jkbarton@caltech.edu, walter.j.chazin@vanderbilt.edu

This PDF file includes:

Figs. S1 to S17
Tables S1 to S2

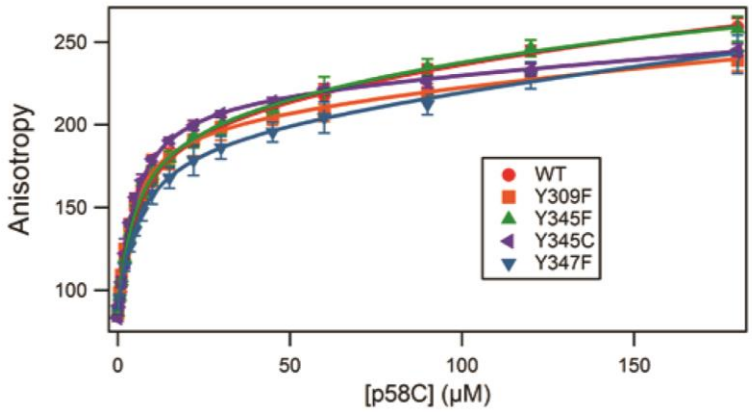

Dissociation constants for p58C

Construct	K_D (μM)
WT	5.5 ± 0.5
Y309F	4.1 ± 0.3
Y345C	4.6 ± 0.2
Y345F	4.9 ± 0.4
Y347F	4.1 ± 0.4

Fig. S1. DNA binding for WT and mutant p58C. WT and mutant p58C domains have similar DNA binding affinities with low micromolar dissociation constants. Affinities were measured in aerobic conditions by fluorescence anisotropy of FITC-labeled DNA substrates in 20 mM MES, pH 6.5, 50 mM NaCl. Background was subtracted from anisotropy values prior to plotting. K_D values are mean ± SD over n=3 measurements for each variant.

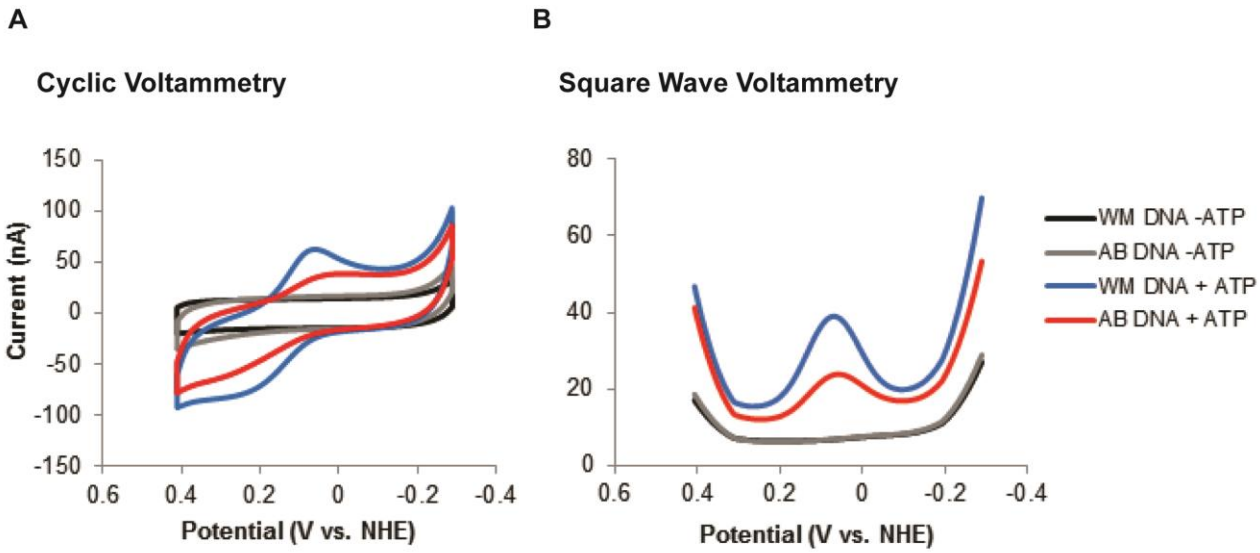

Fig. S2. Cyclic voltammetry (**A**) and Square Wave Voltammetry (**B**) signals of p58C bound to of well-matched (WM) DNA or DNA containing an abasic site (AB DNA) in the duplex segment, in the presence and absence of an NTP pool. The p58C domain displays a reversible redox signal centered at 140-150mV vs. NHE in the presence of ss/dsDNA and 500μM [ATP]. This suggests that the [4Fe4S] cluster in DNA primase is capable of undergoing reversible redox activity when the enzyme is in its active form, bound to DNA and NTPs. All electrochemistry was performed in anaerobic conditions with a Ag/AgCl reference, on 10μM [p58C] in 20mM Tris, pH 7.2, 75mM NaCl. Cyclic voltammetry scan rate: 100mV/s, square wave voltammetry scan frequency: 15 Hz.

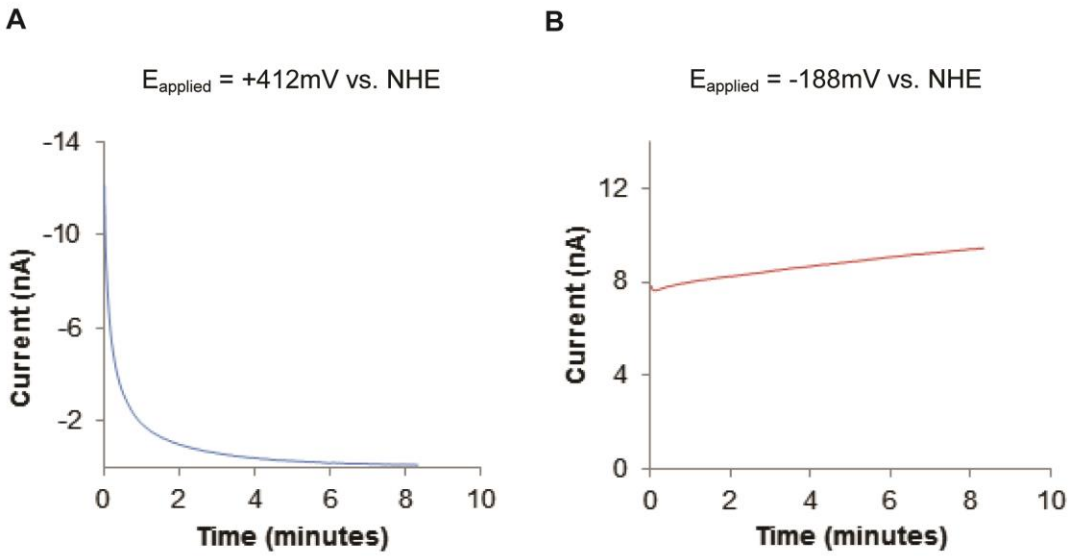

Fig. S3. Oxidation (**A**) and reduction (**B**) of p58C by bulk electrolysis on a DNA-modified multiplex Au electrode. Potentials shown on oxidation/reduction plots were applied to convert the sample at the DNA/solution interface to the desired [4Fe4S] cluster oxidation state. Bulk electrolysis is performed on 16μM p58C using a Ag/AgCl reference electrode, in 20 mM Tris buffer, pH 7.2, 75mM NaCl, in anaerobic conditions.

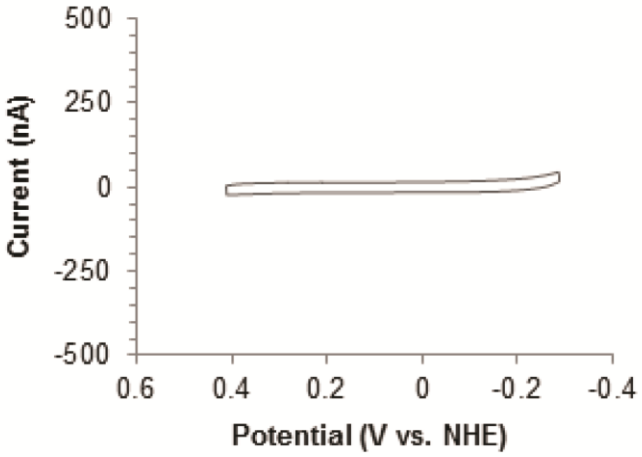

Fig. S4. P58C does not produce a redox signal on ss/dsDNA in the absence of electrochemical alteration. CV performed in anaerobic conditions on 16μM p58C using a Ag/AgCl reference electrode, in 20mM Tris buffer, pH 7.2, 75mM NaCl. CV scans were conducted at a 100mV/s scan rate.

A

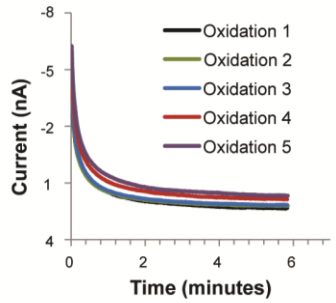

B

Oxidation Step	Cathodic Peak Charge Transfer (nC)
1	65.4
2	112.4
3	116.4
4	151.1
5	170.9

C

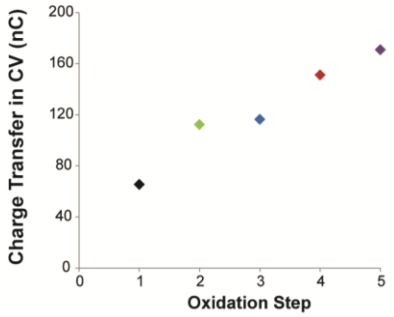

Fig. S5. A) Iterative oxidation reactions on a single DNA-modified multiplex electrode surface. Oxidation reactions of p58C indicate that charge passes, converting a reduced species to an oxidized species at an applied potential of +412mV vs. NHE. This shows that after reduction in CV, p58C can be oxidized again on a DNA-modified surface. **B**) Charge transfer (nC) in the cathodic peak signal for each CV scan of the iteratively oxidized p58C sample. Charge transfer increases during iterative oxidations, due to more p58C available at the DNA/solution interface during later trials. **C**) Plot of CV charge transfer for iterative oxidation steps. Charge transfer in CV peak increases over iterative scans, suggesting that electrochemical oxidation brings more p58C to the ss/dsDNA substrate. Electrochemistry performed on 16μM p58C in 20mM Tris, pH 7.2, 75mM NaCl. CV scans performed at 100mV/s scan rate.

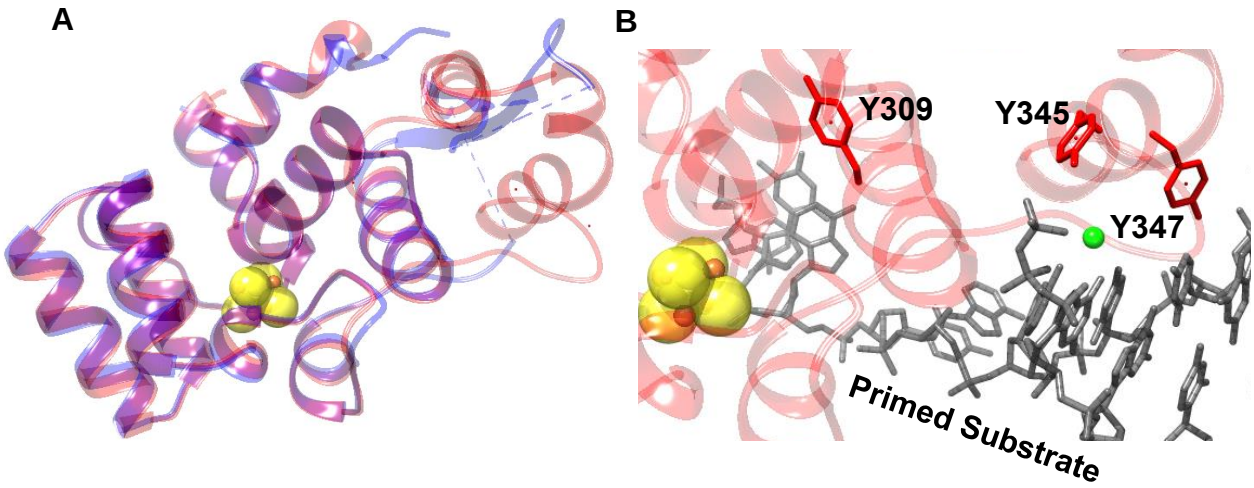

Fig. S6. Comparison of p58C structures obtained with two different crystallization conditions. **A**) Superposition of the two p58C structures, 5F0Q (red) and 3LQ9 (blue). **B**) Expanded region of the 5F0Q structure showing the distribution of the three conserved tyrosine residues that make up the proposed charge transport pathway.

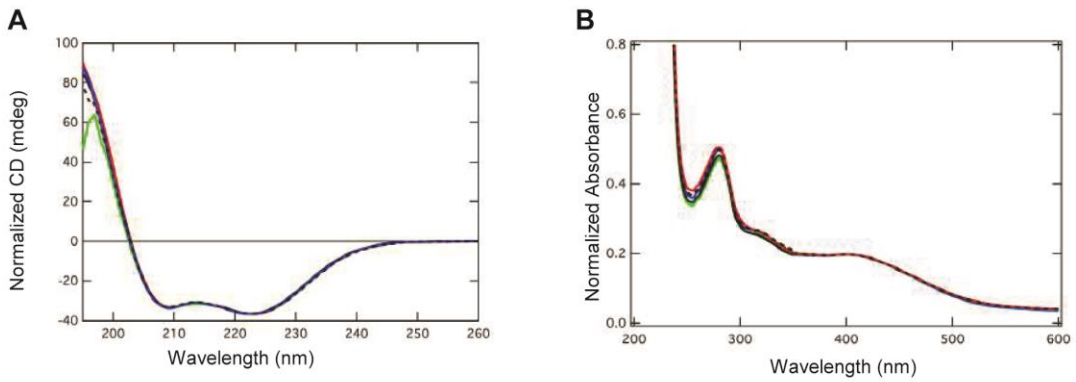

Fig. S7. WT and mutant p58C biophysical characterization. **A**) Circular dichroism (CD) spectroscopy of WT and mutant p58C indicate the mutations do not perturb any of the elements of secondary structure. All spectra normalized to WT at 222 nm. **B**) UV-Visible spectroscopy of WT and mutant p58C shows similar 280 nm/410 nm absorbance ratios, indicating similar degrees of [4Fe4S] cluster cofactor loading in all variants. All spectra normalized to WT at 410 nm.

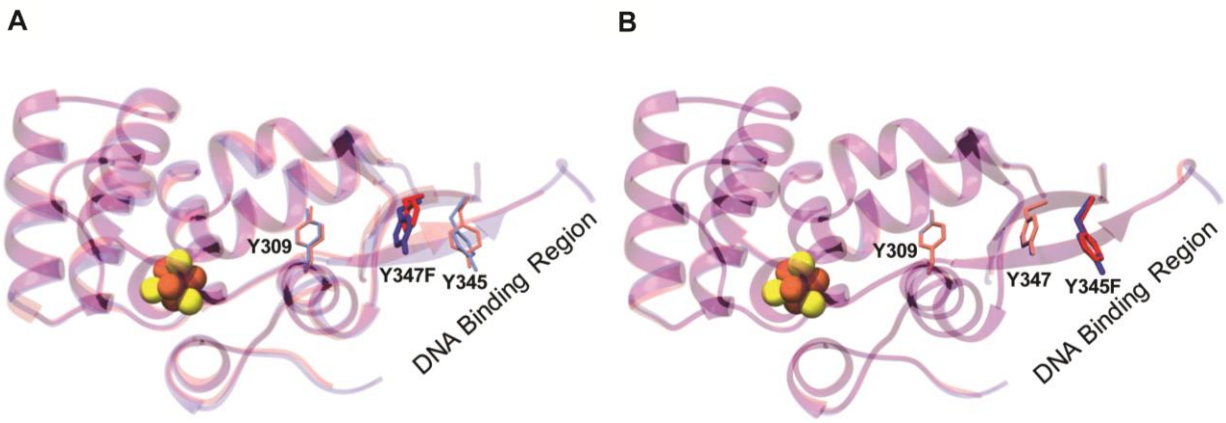

Fig. S8. Structural comparison of WT and mutant p58C. **A**)Superposition of the WT p58C (PDB 3L9Q) and Y347F p58C (PDB 5DQO) structures. **B**) Superposition of the WT p58C (PDB 3L9Q) and Y345F p58C (PDB 517M) structures. In both panels, WT p58C is colored blue and the tyrosine to phenylalanine mutant is red.

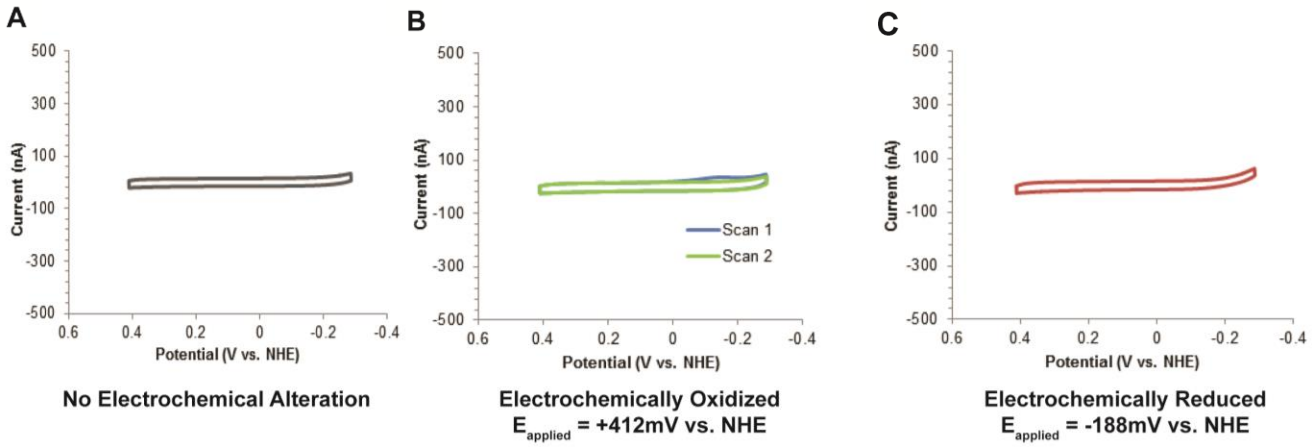

Fig. S9. CV scans of p58C Y345F. **A**) Electrochemically unaltered p58C tyrosine mutants display no electrochemical signal on DNA. **B**) Electrochemically oxidized p58C tyrosine mutants display a cathodic peak between -150mV and -160mV vs. NHE after oxidation at an applied potential of +412mV vs. NHE; the peak signal is smaller than that observed for wild type. **C**) Tyrosine mutants of p58C display no redox signal on DNA after electrochemical reduction at an applied potential of -188mV vs. NHE. All scans performed on 16μM p58C variant, in 20mM Tris, pH 7.2, 75mM NaCl, at a 100mV/s scan rate. P58C Y345F is shown as a representative example of the mutants.

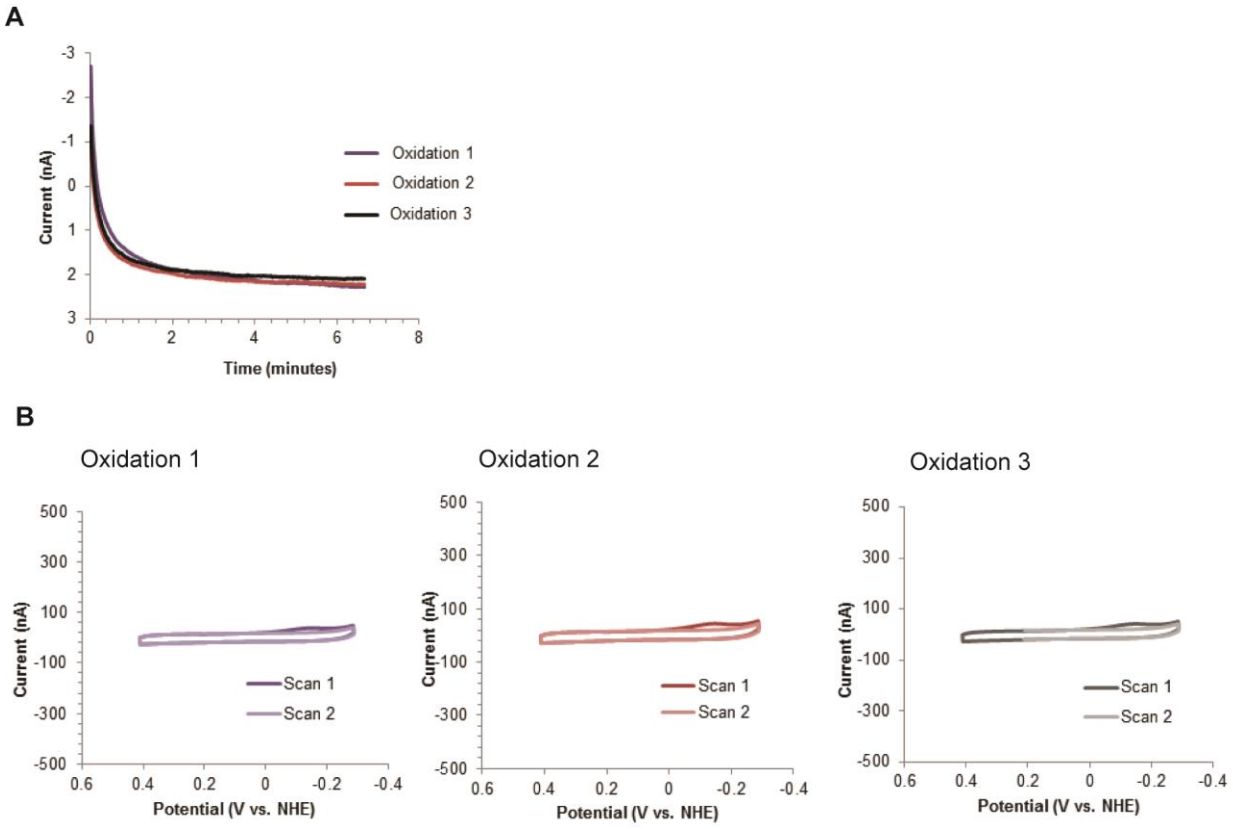

Fig. S10. Iterative Oxidations, followed by CV scans, of p58C Y345F on a single electrode surface. **A**) Three bulk electrolysis reactions at an applied potential of +412mV vs. NHE were performed in immediate succession on a single electrode surface. **B**) CV scans after each successive oxidation. Charge transfer in the cathodic peak was 4.1nC, 5.3nC, and 6.3nC during oxidations 1, 2, and 3, respectively. The mutant p58C thus shows the same general trend as WT but transfers less charge in bulk electrolysis and subsequent CV on the DNA-modified surface. All scans performed on 16μM p58C variant, in 20mM Tris, pH 7.2, 75mM NaCl, at a 100mV/s scan rate. P58C Y345F is shown as a representative example of the mutants.

A

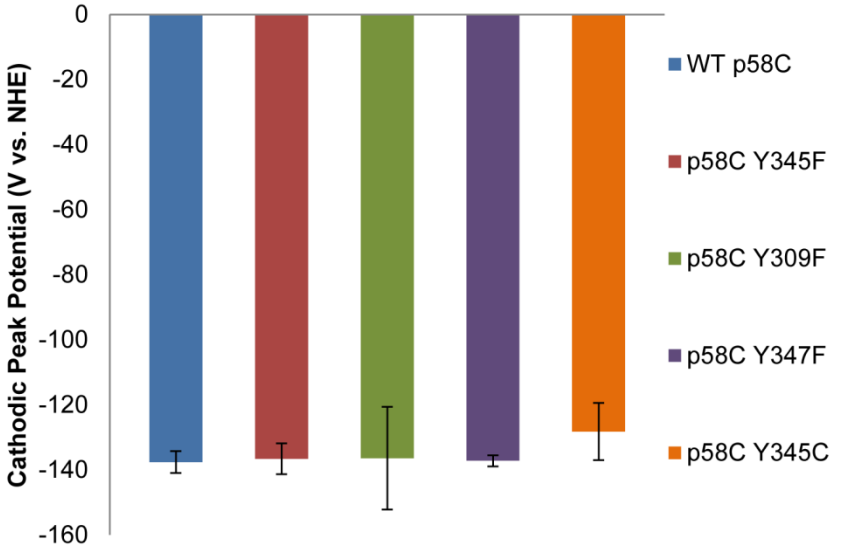

B

	E_{peak} (mV vs. NHE)
WT	-138±3.4
Y345F	-137±4.8
Y309F	-136±16
Y347F	-137±1.7
Y345C	-128±8.7

Figure S11. Change in potential value for cathodic peak after p58C oxidation, WT and tyrosine mutants of p58C. Potential measurements from three CV trials after p58C electrochemical oxidation show that the WT potential is more negative on average, but the difference between WT and mutant p58C cannot be determined to a significant degree outside the margin of error. This suggests that the mutants are more likely to be in the reduced $[4Fe4S]^{2+}$ state than the WT protein with an intact charge transfer pathway, as expected. Potential values are reported as mean ± SD over n= 5 trials.

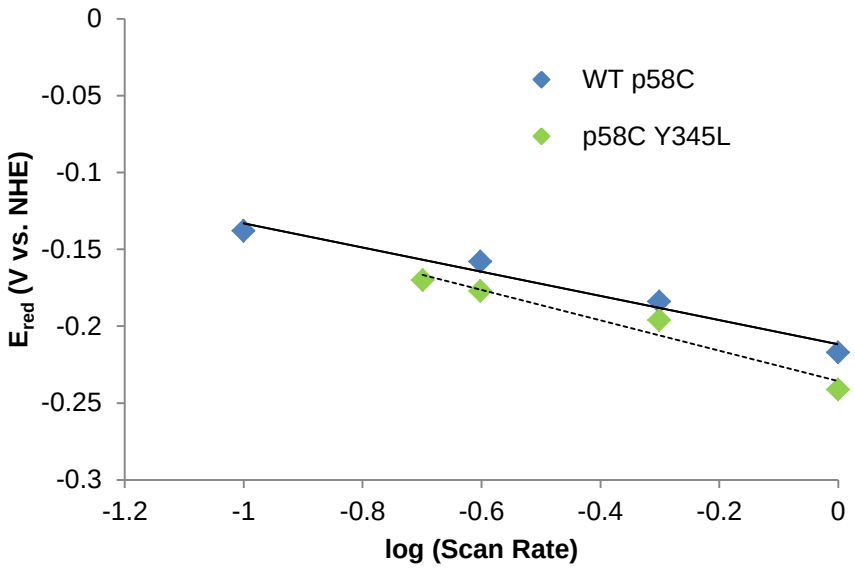

Figure S12. Scan Rate dependence of cathodic peak potential in p58C CV signal after electrochemical oxidation. The peak potential varies with the log of the scan rate for WT p58C (blue points, solid line) and for p58C Y345L (green points, dashed line), as is expected for an irreversible signal (*55*) in CV. The similar linear relationships of the potential and log of the scan rate for these two relationships demonstrate that the rate-determining step in generating this CV signal is tunneling through the alkanethiol linker tethering the DNA substrate to the gold electrode surface.

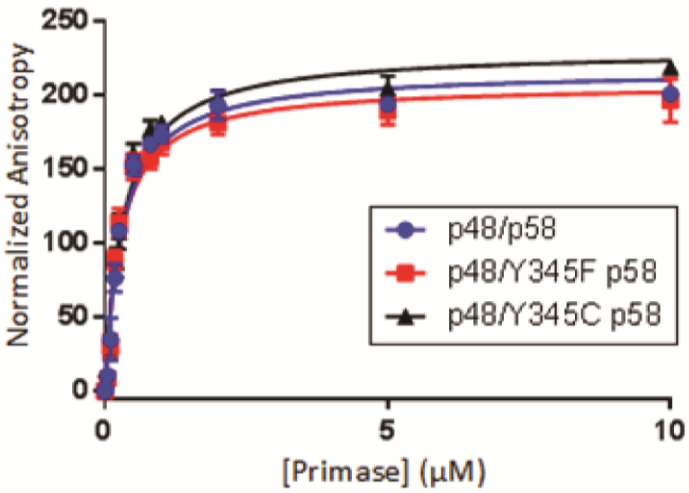

Dissociation Constants for p48/p58

Construct	K_D (μM)
p48/p58	0.30±0.03
p48/p58Y345F	0.28±0.04
p48/p58Y345C	0.32±0.04

Fig. S13. DNA binding for WT and mutant primase. WT and mutant primase have similar DNA binding affinities with high nanomolar dissociation constants. Affinities were measured by fluorescence anisotropy of FITC-labeled DNA substrates in the presence of atmospheric oxygen in 20 mM HEPES, pH 7.5, and 75 mM NaCl. Background was subtracted from anisotropy values prior to plotting. K_D values are mean ± SD over n=3 measurements for each variant.

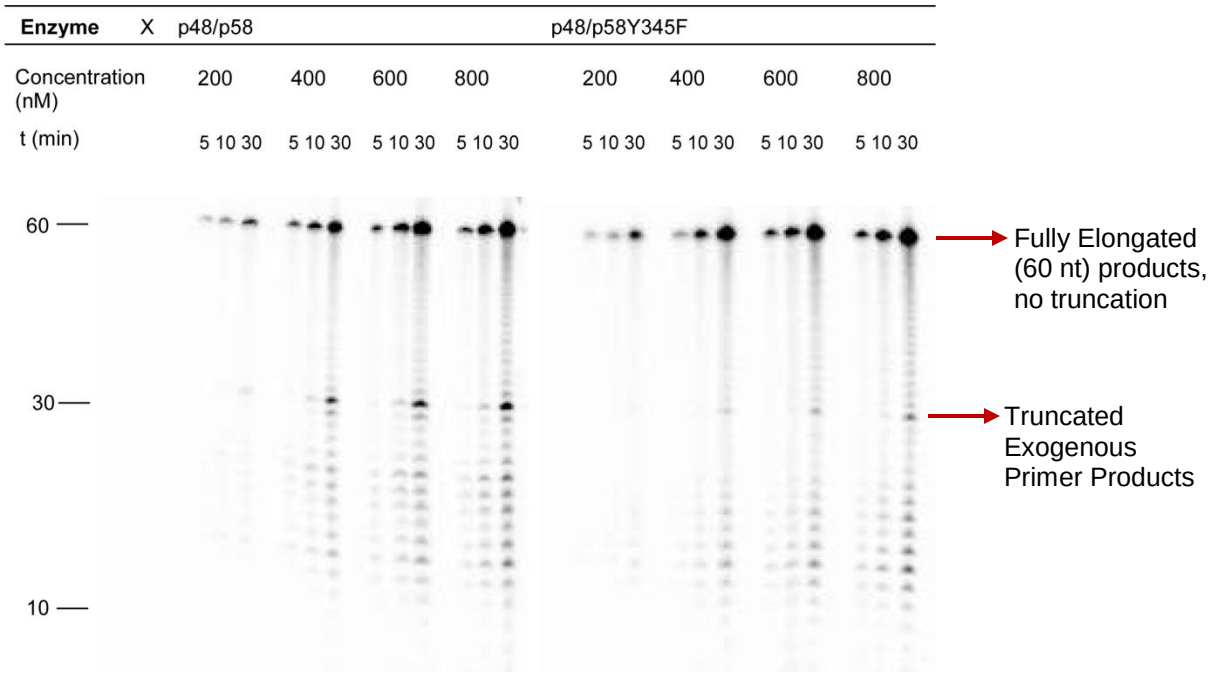

Figure S14. Gel separation of products for elongation reactions with increasing concentrations of p48/p58 and p48/p58Y345F on 2'-OMe RNA-primed DNA. WT primase, which has an efficient redox switching pathway between bound DNA and the [4Fe4S] cluster, synthesizes slightly more truncated products on average. The CT pathway through the protein is important for the redox switch, but it does not appear to be the sole mediator of primase product truncation. Elongation assays were performed anaerobically, with 500nM primed DNA, 1 μM α-^{32}P ATP, 120 μM CTP, 180 μM UTP, 200-800 nM enzyme in 50 mM Tris, pH 8.0, 3 mM $MgCl_2$, at 37 °C.

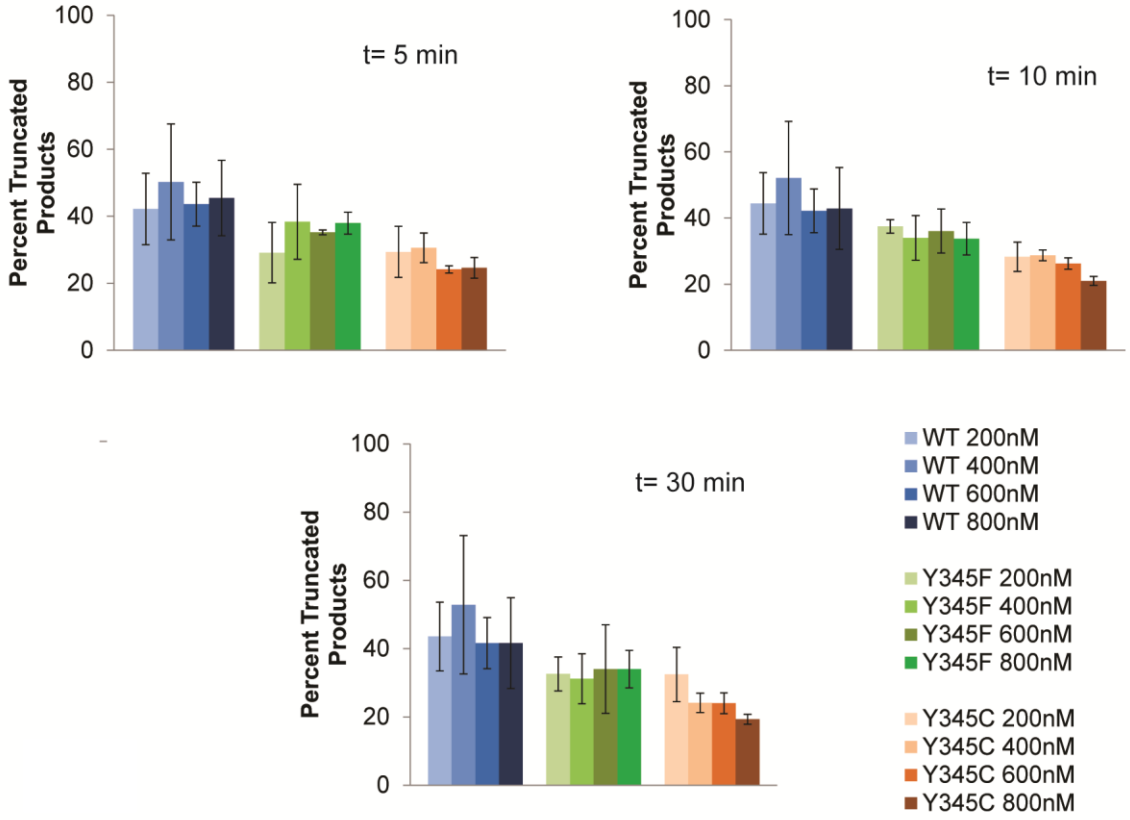

Fig. S15. Percent of primase products truncated by WT and CT-deficient variants at 5, 10, and 30 minutes of incubation at 37°C, under anaerobic conditions. Primase mutants are identified by the mutation in the p58C domain. WT and mutant primase elongation activity at t= 5 minutes (top left), t= 10 minutes (top right), and t= 30 minutes (bottom left) of incubation. Legend is shown on the bottom right. All measurements are mean ± SD for n= 3 trials.

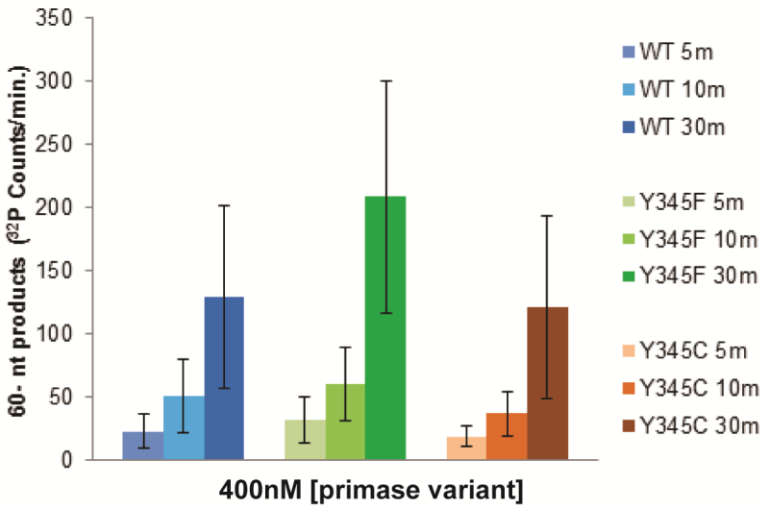

Fig S16. Quantification of 60-nt products synthesized by WT and CT-deficient variants at 5, 10, and 30 minutes of incubation at 37°C, under anaerobic conditions. The products, quantified by calculating ^{32}P counts/minute from α-^{32}P ATP incorporated into products separated by mass on a 20% PAGE denaturing gel, are identical between variants within error for each time point. The 60-nt products were quantified and compared to assess the nucleotide polymerization of each variant, as these products are independent of regulation by the redox switch. This demonstrates that CT-deficient primase retains the ability to polymerize nucleotides and elongate exogenous primers. Conditions are shown for 400nM enzyme concentration reactions. All measurements are mean ± SD for n= 3 trials.

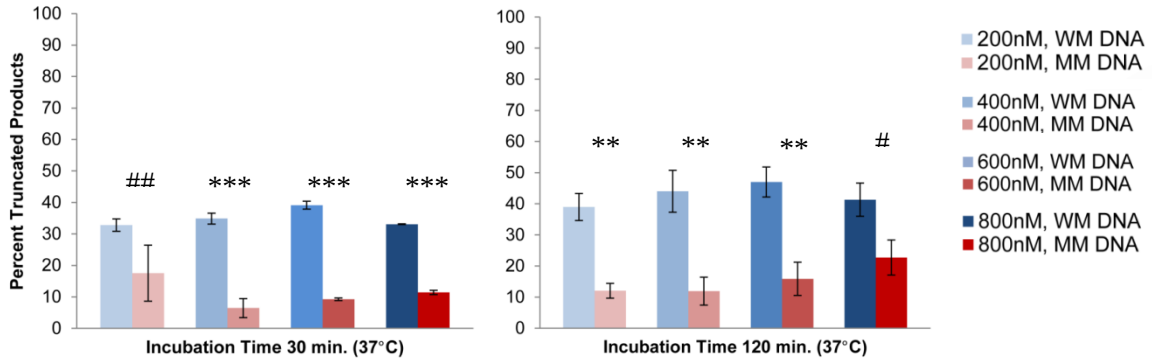

Figure S17. Percentage of WT primase truncated products for a) t = 30 minutes (left) and b) t = 120 minutes (right). Similar to the 60 minute time point (incubation at 37°C), these plots suggest that CT-proficient primase synthesizes significantly more truncated products on well-matched, primed DNA than in the presence of a single base mismatch within the RNA primer. When primase cannot participate in DNA CT, it favors product elongation to primer-multimer length, at all concentrations of CT-proficient primase assayed. Mean ±SD values are plotted for n= 3 trials, # = $0.025<p<0.01$, ## = $0.005<p<0.01$, ** = $0.001<p<0.0005$, *** = $p<0.0005$ (student's t-test).

p58C Electrochemistry Substrates	Well-matched 5'-SH-GTCGTGCAACGTGTCTGCGC-3' 3'-CAGCACGTTGCACAGACGCGTAC-5'	Abasic Site 5'-SH-GTCGTGCAACGTGTCTGCGC-3' 3'-CAG_ACGTTGCACAGACGCGTAC-5'
Initiation Substrate	3'-AAAAAAAAAAAAAAAAAAAAAAAAAATAAAGAGAGAGAGAGAGAGAAAAGA-5'	
Well-Matched Elongation Substrate	3'-(U)$_{16}$(T)$_{15}$-5' 5'-AGAAAAGAGAGAGAGAGAGAGAAAAGAAT(A)$_{31}$-3'	
Mismatched Elongation Substrate	3'-(U)$_{16}$(T)$_{15}$-5' 5'-AGAAAAGAGAGAGAGAGAGAGAACAGAAT(A)$_{31}$-3'	
P58C Fluorescence Anisotropy Substrate	3'-GAGAGTTT-5' 5'-[Flc]-TCTCTCTCTCAAA-3'	
Primase Fluorescence Anisotropy Substrate	5'[Flc]-TTTTTTTTTTTTTTTTTTTTTTTTT-3'	

Table S1. Electrochemistry, primase activity assay, and fluorescence anisotropy DNA substrates used. Electrochemistry of p58C was performed on self-assembling monolayers of a 20-mer DNA duplex substrate with a 3-nt 5'- ssDNA overhang. A 50-nt ssDNA substrate with a single thymine base complementary to the α-^{32}P radiolabeled ATP was used in the primase initiation assay comparing wild type and CT-deficient full-length enzyme. A 2'-OMe RNA-primed ss/dsDNA substrate, containing a 31- nucleotide duplex segment and a 29- nucleotide 5'-ssDNA overhang was used to assay elongation. The mismatched elongation assay was performed with a cytosine engineered into the substrate (red) to promote a mismatch in the elongated primer segment. U = 2'-OMe rU, SH = -$(CH_2)_6$-SH, Flc = FITC

Table S2

Crystallographic data collection and refinement statistics.

PDB Entry	**517M**	**5DQO**
Protein Structure	Y345F	Y347F
Data Collection		
Space Group	C2	P31
Cell dimensions		
a, b, c (Å)	109.9, 52.7, 89.2	60.40, 60.40, 246.73
α, β, γ (°)	90, 115.25, 90	90, 90, 120
Temperature (K)	100	100
Wavelength (Å)	0.987	0.999
Resolution (Å)[a]	49.7-1.93 (1.96-1.93)	44.14- 2.48 (2.53-2.48)
Reflections		
Total	142, 467	184, 871
Unique	35, 604	41, 462
Completeness (%)[a]	99.9 (99.8)	99.1 (89.6)
R_{merge} (%)[a,b]	8.7 (58.4)	5.8 (49.3)
R_{pim} (%)[a]	0.048 (0.33)	2.9 (33.9)
$CC_{1/2}$ (%)[a]	(88.6)	(59.2)
I/σI	18.7 (2.1)	27.6 (2.1)
Redundancy	4.2 (4.0)	4.5 (2.9)
Refinement		
R_{work}/R_{free} (%)[c]	21.0/24.9	24.9/27.4
No. of residues		
Protein	314	628
4Fe-4S	2	4
Solvent	81	41
Average B-Factor (Å)		
Protein	28.8	53.69
4Fe-4S	21.5	46.16
Solvent	27.7	55.66
Wilson B-Factor (Å^2)	24.5	58.1
RMSD Bonds (Å)	0.02	0.02
RMSD Angles (°)	2.11	1.91
Ramachandran (%)		
Most favored	99%	98.5%
Allowed	1%	1.5%
Disallowed	0%	0%

[a] Values in parentheses are for the highest-resolution shell. [b] $R_{merge} = \Sigma(|I-\bar{I}|)/\Sigma I \times 100$. [c] $R_{work} = \Sigma |F_o-F_c|/\Sigma F_o \times 100$, where F_o is the observed structure factor amplitude and F_c is the calculated structure factor amplitude.

Table S2. Crystallographic Data for p58C Y345F (PDB 517M) and p58C Y347F (PDB 5DQO).